FEBS Letters 589 (2015) 2304–2311

FEBS Letters

journal homepage: www.FEBSLetters.org

# Mathematical modeling reveals a critical role for cyclin D1 dynamics in phenotype switching during glioma differentiation

Xiaoqiang Sun [a,b,*], Xiaoke Zheng [c,1], Jiajun Zhang [b], Tianshou Zhou [b], Guangmei Yan [d], Wenbo Zhu [d,*]

[a] Research Center of Bioinformatics, Zhong-shan School of Medicine, Sun Yat-Sen University, Guangzhou 510089, China
[b] School of Mathematical and Computational Science, Sun Yat-Sen University, Guangzhou 510000, China
[c] First Affiliated Hospital of Sun Yat-Sen University, Guangzhou 510000, China
[d] Department of Pharmacology, Zhong-shan School of Medicine, Sun Yat-Sen University, Guangzhou 510089, China

ARTICLE INFO

*Article history:*
Received 11 April 2015
Revised 8 July 2015
Accepted 13 July 2015
Available online 17 July 2015

Edited by Paul Bertone

*Keywords:*
Phenotype switching
Cyclin D1
Glioma differentiation
Mathematical modeling

ABSTRACT

**Glioma differentiation therapy is a novel modality to increase anti-glioma effects using specific drugs to induce glioma cell differentiation to glia-like cells. However, the molecular mechanisms underlying glioma differentiation remain poorly understood. In this study, we built an experiment-integrated mathematical model for glioma differentiation signaling pathways. Our modeling and experimental analysis revealed that a "one-way-switch" bifurcation of cyclin D1 dynamics was critical for controlling the phenotypic transition of glioma cells. We also quantitatively evaluated drug combinations toward a synergistic therapeutic effect. These results provide insights into the molecular mechanisms underlying glioma differentiation and implications for the design of novel therapeutic targets in anti-cancer therapy.**


## 1. Introduction

Malignant gliomas are one of the most complex deadly cancers worldwide. Traditional therapy with surgery, radiation, and chemotherapy rarely cure the disease [1]. Differentiation therapy is a novel promising strategy to increase anti-glioma effects using specific agents to modify glioma cell differentiation [2]. Recent reports have shown that cholera toxin (a type of biotoxin) can induce glioma cell differentiation [3]. However, the molecular mechanisms underlying glioma differentiation remain poorly understood [4].

Our recent study showed that cholera toxin (CT), a well-known inducer of cAMP activity [5], induced glioma cell differentiation. Based on these observations, we hypothesized that cAMP/PKA signaling played important roles in the induced differentiation of glioma cells. Our experiment demonstrated that PKA-mediated cAMP signaling phosphorylated CREB at Ser-133 [3], which was required for cholera toxin-induced differentiation. cAMP/PKA signaling can also inhibit the PI3K/AKT pathway that phosphorylates GSK3β into its inactive form. The increased activation of GSK3β also contributes to cholera toxin-induced differentiation [6]. GSK-3β has been shown to trigger cyclin D1 nuclear export and its subsequent degradation [6], which is required for glioma cell differentiation. Additionally, the IL-6/JAK2/STAT3 pathway was demonstrated to be involved in cholera toxin-induced differentiation of glioma cells [7].

To extend the analysis of interactions between drug stimulation and glioma differentiation beyond a single linear pathway, we designed a systems biology approach to study key components and interactions involved in various signaling pathways that control phenotype switching of glioma cells between differentiation and proliferation.

Several mathematical and computational models of cell fate decision have been developed. Gérard et al. [8] proposed a computational model for the cyclin-dependent kinases (CDKs) network, which controls the dynamics of the mammalian cell cycle, to investigate how the regulatory structure of the CDKs network results in its temporal self-organization. Yao et al. [9] built an ordinary differential equations (ODEs) model of the cyclin D/CDK-Rb–E2F pathway and revealed a bistable switch of E2F that underlays the restriction point, which is critical for the proliferation of

*Author contributions:* Conceived the project: XS. Designed the experiments: XS and WZ. Developed the mathematical model: XS. Performed the experiments: XZ. Contributed reagents/materials/analysis tools: GY. Wrote the paper: XS. Revised the paper: XS, XZ, and WZ. Participated in discussion: XS, XZ, JZ, TZ, and WZ.

* Corresponding authors at: Research Center of Bioinformatics, Zhong-shan School of Medicine, Sun Yat-Sen University, Guangzhou 510089, China (X. Sun).

*E-mail addresses:* xiaoqiangsun88@gmail.com (X. Sun), zhuwenbo@mail.sysu.edu.cn (W. Zhu).

[1] Shared first author.

http://dx.doi.org/10.1016/j.febslet.2015.07.014
0014-5793/

mammalian cells. Then, the bistable E2F accumulation was tested experimentally. However, no models have been developed to examine the regulatory mechanisms controlling the phenotype transition of glioma cells between proliferation and differentiation.

In the present study, we used a systems biology approach to investigate the molecular mechanisms controlling the differentiation of glioma cells. First, we built an ODEs model of the signaling pathways involved in drug-induced glioma differentiation. Experimental data were used to fit and validate the model. Then, we performed sensitivity analysis and bifurcation analysis for the developed system. The model analysis revealed that a "one-way-switch" bifurcation of cyclin D1 controlled the transition of the glioma cell phenotype from proliferation to differentiation. Moreover, the critical role of cyclin D1 in controlling glioma cell phenotype switching was tested experimentally. We also discussed drug combinations toward a synergistic therapeutic effect. These results provide insights into the molecular mechanisms underlying glioma differentiation and suggest potential therapeutic targets and the benefit of combining drugs for glioma chemotherapy.

## 2. Results

### 2.1. Experiment-integrated mathematical modeling of the signaling pathways involved in drug-induced glioma differentiation

Our previous experiments [3] showed that cholera toxin elevated cAMP signaling in glioma cells and triggered morphologic transformations in almost all glioma cells after treatment with 10 ng/ml cholera toxin for 48 h. Furthermore, a dose-dependent effect of cholera toxin showed that GFAP expression increased abruptly when the cholera toxin dose passed a threshold of 7.5–10 ng/ml. A steep rise in the response to increasing external stimulation within a narrow range is characteristic of "ultrasensitivity" in the dose–response relationship [10,11]. The feature of an all-or-none response and ultrasensitivity may characterize bistability or a bifurcation switch [12,13]. We explored the mechanism underlying this interesting phenomenon by quantitatively studying the drug-induced differentiation of signaling pathways in glioma cells.

We modeled these signaling pathways by employing a set of ODEs (Eqs. (2)–(12) in Section 4). Hill functions [14–16] were employed to describe regulatory relationships between proteins in the signaling pathways. As indicated in our previous experimental data (Table S1), cyclin D1 activation showed an ultrasensitive response to cholera toxin treatment. Therefore, a non-linear positive feedback of cyclin D1 activation (e.g., through cyclin D auto-activation [21] or the cyclin D/CDK4-6/Rb/E2F/cyclin D feedback loop [8,17]) was assumed in our mathematical model (see details in Section 4). This assumption was also inspired by parameter fitting as described below.

The unknown parameters in the model were fitted to the experimental data [3,6,7] (Table S1) using an optimization procedure (see Text S1 for detailed methods). Our data include both time series data and different treatment condition data. A modified genetic algorithm associated with an ODE solver was designed to integrate and fit these two types of data. The estimated parameter values are listed in Table S2. Fig. 2 compares the simulation results with the experimental data (mean squared error = 0.1384). The Pearson correlation coefficients were also calculated to quantify the closeness between the simulated and experimental data, as shown in Fig. 2. The complete results of parameter estimation are listed in Fig. S1. These results demonstrated that the simulation results of the model with the estimated parameters are consistent with the experimental data. Moreover, we found that the model without feedback of cyclin D1 did not fit the experimental data well, which demonstrated the rationality of the model assumption described above.

We further validated the model with another sample of experimental data [3,6]. Fig. 3 shows the experimental validation for predicted GFAP and PCNA activation at different time points or under different treatment conditions. Fig. 3A validates the dose response of GFAP to cholera toxin (0, 5, 7.5 and 10 ng/ml); Fig. 3B compares the time course of GFAP under treatment with cholera toxin (10 ng/ml) on different days (days 0, 1, 2, 4 and 6) using the experimental data. Validations of the GFAP and PCNA levels under different conditions (GSK-3β gene silencing mediated by siRNAs and cyclin D1 degradation inhibition using MG132) are shown in Fig. 3C and D, respectively. The good agreement between the simulations and experimental data confirmed that our model accurately reflected the dynamics of the signaling pathways and thus could be used to predict the glioma cell's states of differentiation and/or proliferation.

We noted that the GFAP level showed a plateau and a subsequent sharp jump in response to increasing cholera toxin in the range of 5–7.5 ng/ml (Fig. 3A). Therefore, we performed a more detailed analysis of the dose response of GFAP to 5–7.5 ng/ml of cholera toxin and the time course (0–48 h) to further understand this interesting "running jump" phenomenon, as presented in Fig. S2.

### 2.2. Bifurcation of cyclin D1 controls the glioma cell's phenotypic transition from proliferation to differentiation

Sensitivity analysis was performed for the estimated parameters (see Text S1 for detailed methods) to investigate which parameters in the model were more sensitive or critical during glioma differentiation. In our analysis, the dose of cholera toxin was increased from 10 to 100 ng/ml. In each case, each parameter was increased by 1% from its estimated value; then, we obtained the time-averaged percentage change of each variable value. When the dose of cholera toxin was small (less than 10 ng/ml), none of the sensitivity values were more than 5% (Fig. 4). However, when the dose of cholera toxin was increased up to 100 ng/ml, some sensitivity values increased up to 10%, indicating that the dynamic activation of some proteins in the signaling pathways changed dramatically. The sensitivity analysis result indicated that the cAMP-increasing drugs could increase the kinetic sensitivities of some proteins involved in the signaling pathways. Moreover, cyclin D1-associated parameters were found to be more sensitive in response to the increased drug doses compared to the other parameters.

Next, we performed bifurcation analysis for cyclin D1 to investigate its dynamics. An irreversible "one-way switch" of decreased cyclin D1 activation was revealed (Fig. 5). The cyclin D1 level was high until the dose of cholera toxin exceeded a critical threshold dose, at which point cyclin D1 decreased abruptly to a low value. Then, the cyclin D1 remained low if the dose of cholera toxin decreased rather than returning to a high level. When the dose of cholera toxin was between 0 and the threshold, the cyclin D1 signaling system was "bistable" [i.e., it had two stable steady-states (the solid lines on the upper and lower branches) separated by an unstable steady state (the dashed line on the intermediate branch)]. The irreversible switch of cyclin D1 is consistent with the proliferation inhibition feature of differentiated glia-like cells induced by cholera toxin.

We investigated the function of cyclin D1 bifurcation in regulating cell phenotype switching by examining its correlations with the differentiation marker GFAP and proliferation marker PCNA. Fig. 6 shows the dose responses of cyclin D1, GFAP and PCNA

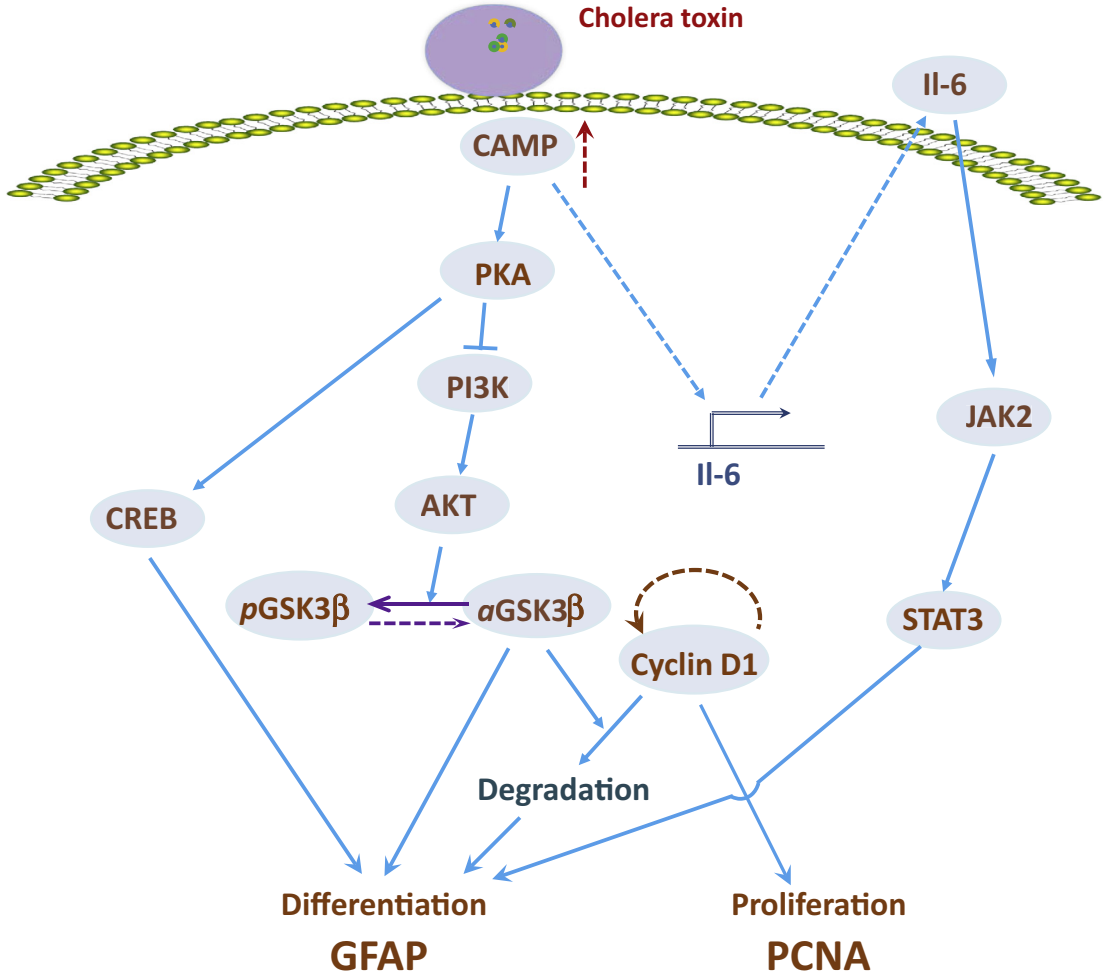


**Fig. 1.** Drug-induced differentiation signaling pathways in glioma cells. cAMP/PKA signaling plays important roles in the differentiation of glioma cells, which can be elevated by cholera toxin (CT; a type of biotoxin). PKA-mediated cAMP signaling can phosphorylate CREB at Ser-133 [3], which is required for cholera toxin-induced differentiation. cAMP/PKA signaling can also inhibit the PI3K/AKT pathway that phosphorylates GSK3β into its inactive form. The increased activation of GSK3β also contributes to cholera toxin-induced differentiation [6]. Furthermore, GSK-3β triggers cyclin D1 nuclear export and its subsequent degradation [6], which is required for differentiation in glioma cells. The IL-6/JAK2/STAT3 pathway is also demonstrated to be involved in cholera toxin-induced differentiation of glioma cells [7]. GFAP and PCNA are reliable differentiation and proliferation markers of glioma cells, respectively.

(evaluated at 48 h) to cholera toxin (0–10 ng/ml) and their temporal dynamics. The changes in GFAP and PCNA were closely correlated with cyclin D1. The dynamic switch of cyclin D1 from "ON" (high level) to "OFF" (low level) triggered GFAP from low to high and PCNA from high to low. These results demonstrated that cyclin D1 might function as a "bio-switch" that controls glioma cell phenotype switching between proliferation and differentiation.

### 2.3. Experimental validation

Experiments were performed to test the critical role of cyclin D1 in controlling differentiation and proliferation in glioma cancer cells. RNA silencing of cyclin D1 was accomplished in C6 cells (see Section 4). After treatment for 48 h, 3 fragments remarkably reduced the level of cyclin D1 protein; the #3 fragment showed the best silencing effect (Fig. 7A). After exposure to cyclin D1 siRNA for 48 h, the flat polygonal shapes of C6 cells were transformed into shrunken cell bodies (Fig. 7B) consistent with the astrocyte-like shape induced by cholera toxin. To verify the dominant role of cyclin D1 in controlling phenotype switching from proliferation to differentiation in C6 cells, we evaluated the protein expression of the differentiation marker GFAP and the proliferation marker PCNA after cyclin D1 silencing. As shown in Fig. 7C, the GFAP protein was increased and PCNA was decreased when cyclin D1 protein was decreased with a time line from 6 h to 48 h. Fig. 7D demonstrates the dose responses of GFAP and PCNA to cyclin D1 siRNA at concentrations ranging from 12.5 to 100 nM. GFAP was unltrasensitively induced by cyclin D1 siRNA at a concentration between 0 and 12.5. The tendency of the PCNA protein level was completely in step with cyclin D1, which showed good agreement with the model prediction in Fig. 6. Full-length blots of Fig. 7A, C and D were provided in Figs. S3 and S4, respectively.

### 2.4. Quantitative evaluation of the synergistic effects of drug combinations

Currently, several inhibitors that target the signaling network involved in this study are in clinical trials, including PI3K inhibitors (e.g., LY294002 (LY), CAL-101, BKM120, and GDC-0941), STAT3 inhibitors (e.g., ISIS-STAT3$_{Rx}$ and OPB-31121) and cyclin D1 inhibitors (e.g., Fascaplysin).

The inhibition effects of these inhibitors were incorporated into our model by multiplying a type of inhibition Hill function into the corresponding equations. Fig. 8 shows the dose responses of combined CT&LY, CT&cyclin D1-inhibitor, and CT&STAT3-inhibitor as well as the combination of the cyclin D1-inhibitor and

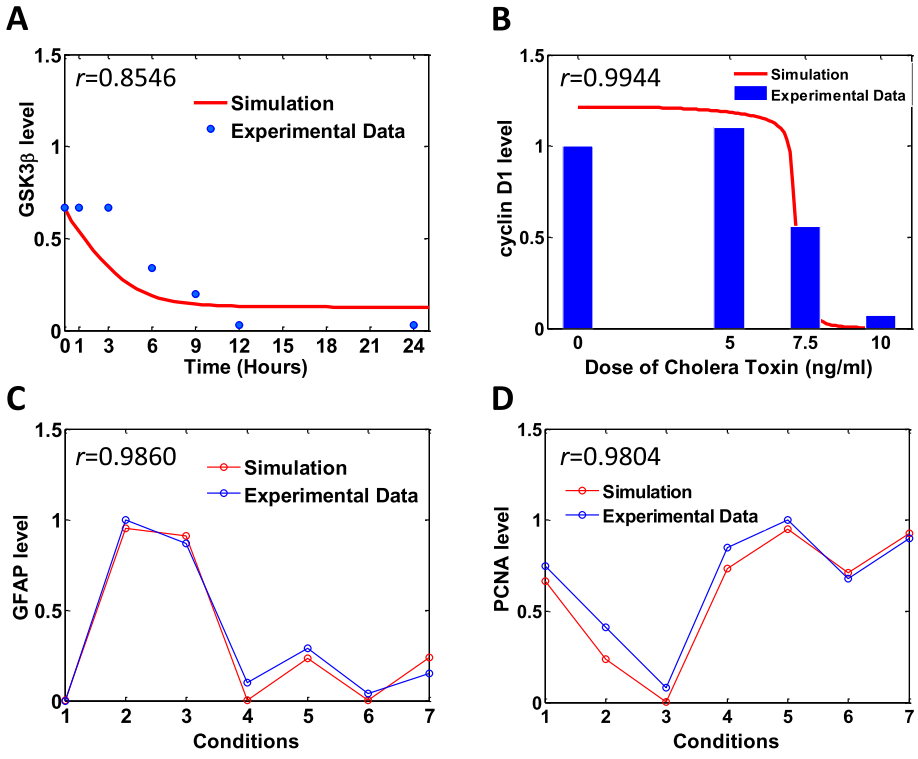


**Fig. 2.** Simulation results of activation levels of several proteins at different time points and/or under different conditions compared to experimental data. Conditions 1–7 correspond to different treatments (see Table S1). The mean squared error between the simulated data and experimental data is 0.1384. The Pearson correlation coefficients ($r$) were also calculated for each pair of simulated and experimental data to analyze the closeness between them.

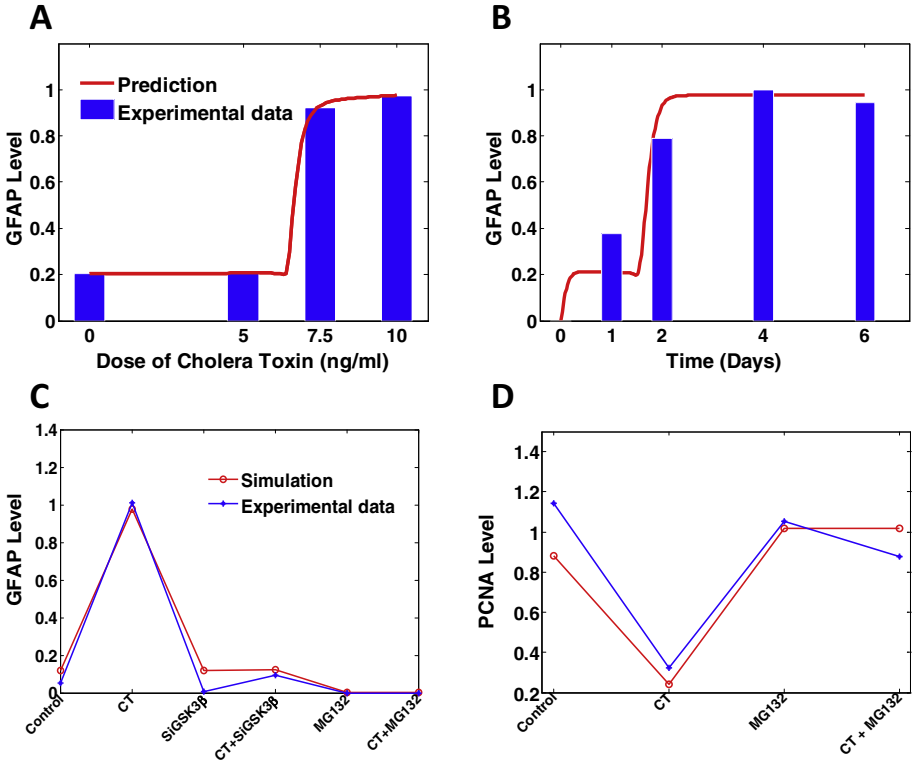


**Fig. 3.** Experimental validation for predicted GFAP and PCNA activation. (A) GFAP levels at different doses of cholera toxin (0, 5, 7.5 and 10 ng/ml); (B) GFAP levels under treatment with cholera toxin (10 ng/ml) on different days (days 0, 1, 2, 4 and 6). (C) GFAP levels under different conditions (GSK-3β gene silencing mediated by siRNAs and cyclin D1 degradation inhibition using MG132). (D) PCNA levels under different conditions involving interfering with cyclin D1 degradation using MG132.

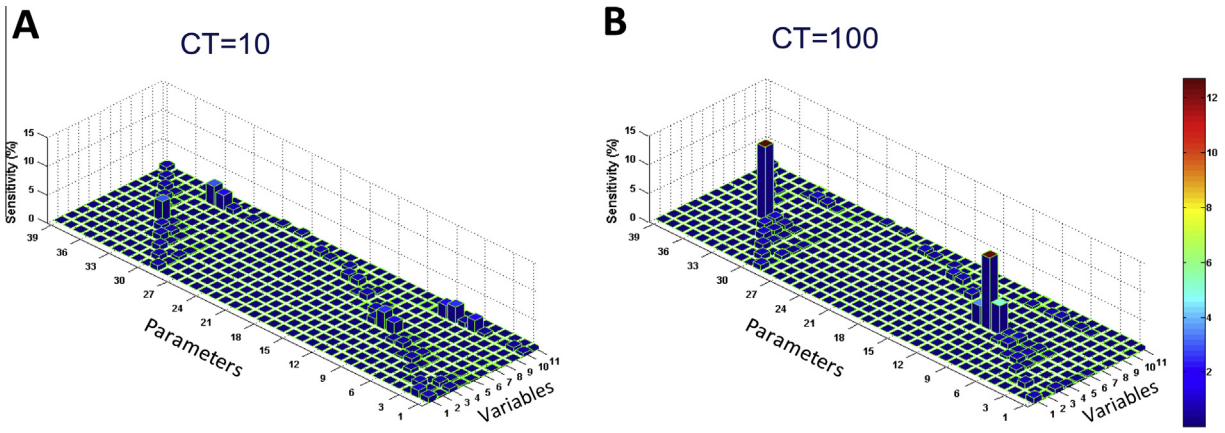


**Fig. 4.** Sensitivity analysis for the constructed system. Proteins 1–11 correspond to variables in Eqs. (2)–(12); parameters 1–39 were listed in Table S1. Each parameter was increased by 1% from its estimated value; then, we obtained the time-averaged percentage change of each variable value. Increased doses of cholera toxin increased the kinetic parameter sensitivities, especially for cyclin D1.

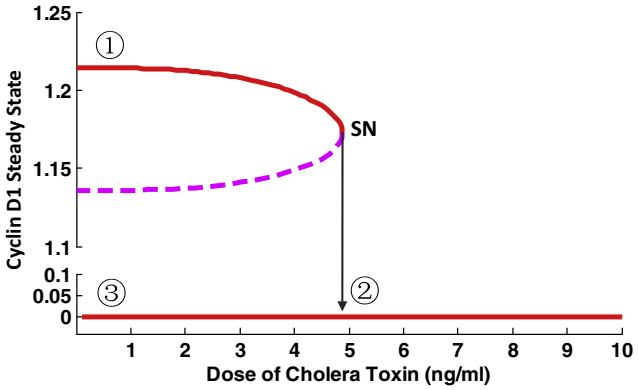


**Fig. 5.** Bifurcation analysis of cyclin D1. Bifurcation diagram for cyclin D1 with respect to doses of cholera toxin shows irreversible "one-way switch" of cyclin D1 activity.

STAT3-inhibitor. Among these combinations, the cyclin D1-inhibtor and STAT3-inhibitor showed the most significant anti-cancer effect by promoting the differentiation and inhibiting the proliferation of glioma cells.

To examine whether the combination of the cyclin D1-inhibtor and STAT3-inhibitor had a synergistic effect, we adopted the Bliss combination index [18,19] as follows:

$$CI_{\text{Bliss}}(x,y) = \frac{R_1(x) + R_2(y) - R_1(x)R_2(y)}{R_{12}(x,y)}, \quad (1)$$

where $R_i(x)$ is the ratio of the normalized level of differentiation to proliferation of glioma cells induced by the inhibitor or drug $i$. $R_1(x) + R_2(y) - R_1(x)R_2(y)$ in Eq. (1) is the expected response effect, and $R_{12}(x,y)$ is the actual combination effect. Hence, the index evaluates the combination as a synergistic effect if $CI < 1$, antagonistic if $CI > 1$, and otherwise is additive. The model predicted that the combinations of the cyclin D1-inhibtor and STAT3-inhibitor resulted in dose-dependent synergism (Fig. 9). The higher their combined dosages, the more synergy they preserved.

## 3. Discussion

In this study, we adopted a systems biology approach to study the molecular mechanisms underlying glioma differentiation therapy. Our model successfully captured the key kinetics of the signaling pathways using both time series data and different treatment condition data. The sensitivity analysis demonstrated that cyclin D1 was a critical component in the signaling networks, and further bifurcation analysis revealed that a "one-way-switch" bifurcation of cyclin D1 controlled glioma cell phenotype switching from proliferation to differentiation.

Many experimental studies [20] have shown that cyclin D1 serves as a switch to regulate the continuation of cell cycle progression [21]. Guided by experiments, in this study a data-driven modeling approach revealed that cyclin D1 controlled the phenotype transition of glioma cells from proliferation to differentiation. In ongoing work, we are further surveying the proteins that up-regulate cyclin D1 expression or activation [22,23] in a detailed

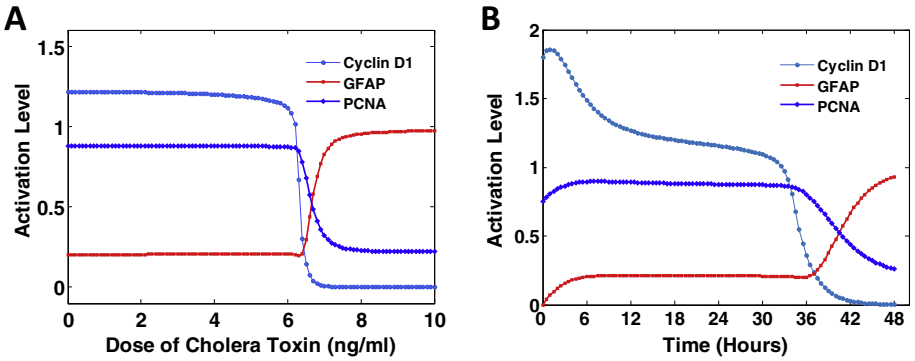


**Fig. 6.** Model prediction of glioma cell phenotype switching from proliferation to differentiation controlled by cyclin D1. (A) Dose-dependent responses and (B) temporal dynamics of cyclin D1, GFAP and PCNA in response to cholera toxin (10 ng/ml). The simulation demonstrated that the switch of cyclin D1 from "ON" (high level) to "OFF" (low level) determined glioma cell phenotype switching from proliferation (high PCNA level) to differentiation (high GFAP level) in cholera toxin induced-differentiation therapy.

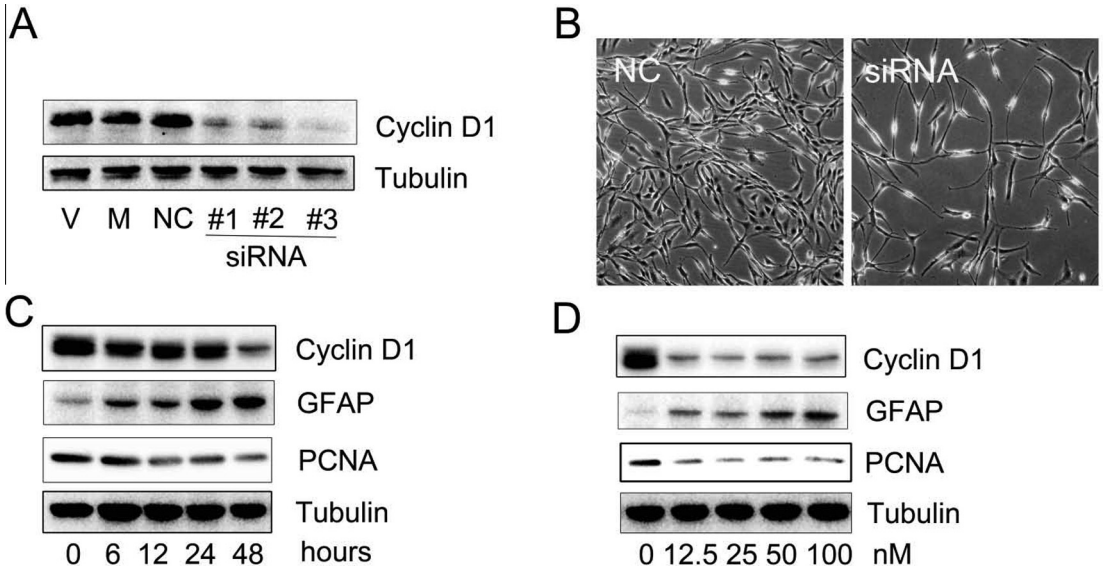


**Fig. 7.** Experimental validation of the critical role of cyclin D1 dynamics in controlling phenotype switching from proliferation to differentiation. (A) Immunoblot of cyclin D1 protein levels after transfection with cyclin D1 siRNA for 48 h. Morphology (B) and immunoblot of the time course (C) and dose responses (D) of cyclin D1, GFAP and PCNA levels in cyclin D1 knockdown cells.

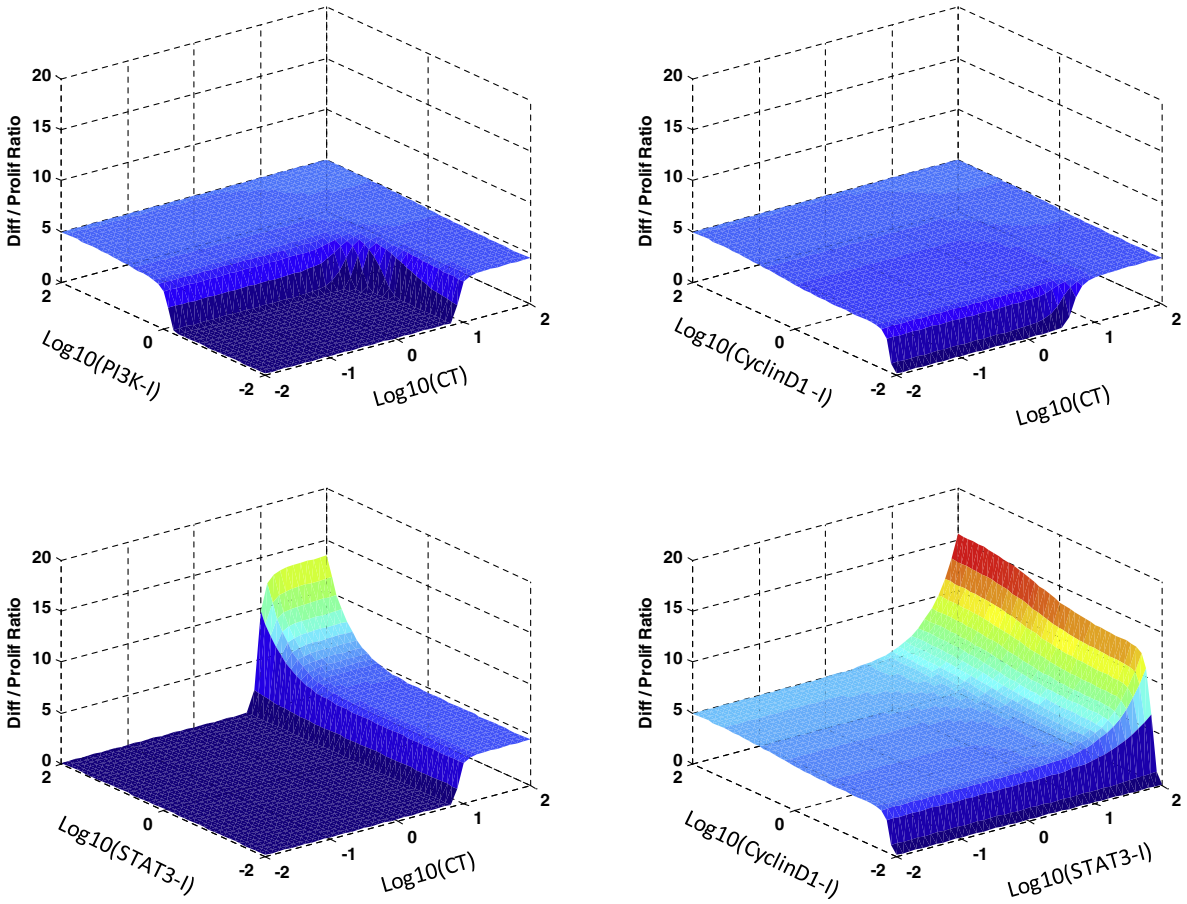


**Fig. 8.** Dose responses of drug combinations. Among these combinations, the cyclin D1-inhibtor and STAT3-inhibitor showed the highest anti-cancer effect by promoting the differentiation and inhibiting the proliferation of glioma cells.

feedback loop. The identification of these proteins would provide us with a better understanding of the mechanisms of resistance to cyclin D1 inhibition. Furthermore, these regulators could be targeted in combination with cyclin D1 inhibition therapy to reduce drug resistance [24] and induce a synergistic therapeutic effect.

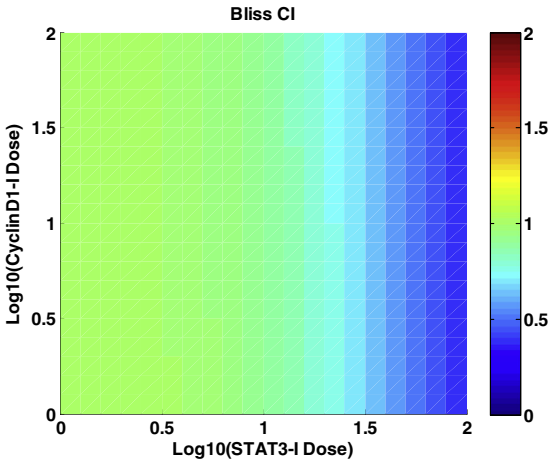


**Fig. 9.** Synergy evaluation of the cyclin D1-inhibtor and STAT3-inhibitor. The model predicted that the combination of the cyclin D1-inhibtor and STAT3-inhibitor performed dose-dependent synergism.

The signaling pathways of glioma differentiation induced by agents in this study were constructed from the experimental evidence established previously. The inference of the signaling pathway or signaling network involved in glioma differentiation from multi-omics data is a vital task but is beyond the scope of this study. In future work, we will link the signaling pathways inferred from the experimental data to the phenotype of cell differentiation and proliferation and build a multiscale model [25–27] incorporating the experimental data at both the molecular and cellular level to evaluate drug synergism and optimize drug doses [28,29].

In summary, we explored the "one-way switch" bifurcation of cyclin D1 that controls phenotype switching from proliferation to differentiation in glioma cancer cells through an integration of experimental data and a mathematical model of the signaling pathways involved in glioma differentiation.

## 4. Materials and methods

### 4.1. RNA silencing of cyclin D1

siRNA fragments (Sigma, St. Louis, Mo, USA) targeting rat cyclin D1 were used to deplete the expression of the corresponding genes. C6 cells were transfected with cyclin D1 siRNA at the indicated concentrations and times using the Lipofectamine™ RNAiMAX reagent (Invitrogen, Carlsbad, CA, USA). The efficiency of knockdown was evaluated by western blotting using an anti-cyclin D1 antibody (1:1000, Cell Signaling Technology, Beverly, MA, USA)

### 4.2. Western blot analysis

C6 cells were cultured in 35 mm plates. At 12 h after seeding, the cells were treated with cyclin D1 siRNA at different concentrations and times; then, total protein was extracted with M-PER (Mammalian Protein Extraction Reagent, Pierce, Rockford, IL, USA) according to the manufacturer's instructions. After measurement of the protein concentration with a BCA Protein Assay Kit (Pierce, Rockford, IL, USA), equal amounts of protein samples were combined with concentrated sodium dodecyl sulfate (SDS) loading buffer, heated at 95 °C for 5 min, and separated by sodium dodecyl sulfate–polyacrylamide gel electrophoresis (SDS–PAGE) prior to Western blotting. Primary antibodies targeting cyclin D1 (1:1000), GPAP (1:1000), PCNA (1:5000, Cell Signaling Technology, Beverly, MA, USA) and Tubulin (1:5000, Sigma) were used in this study. After incubation with a horseradish peroxidase-labeled secondary antibody (1:1000, Cell Signaling Technology, Beverly, MA, USA), the visualization of protein was accomplished with the enhanced chemiluminescence detection system (Pierce, Rockford, IL, USA) and an immunoblotting imaging and analysis system (BioRad, CA, USA).

### 4.3. ODEs modeling

We used a system of ODEs to model the signaling pathways induced by cholera toxin (shown in Fig. 1). Michaelis–Menten kinetics and Hill functions were employed to describe regulatory relationships within the signaling network given that the less critical reaction details were simplified.

Cholera toxin induced-phosphorylation of PKA, CREB, PI3K, AKT and GSK3β upstream of the signaling pathway was described by the following Eqs. (2)–(6).

$$\frac{d[\mathrm{PKA}]}{dt} = a_1 + \frac{V_1 \cdot CT^{n_1}}{K_1 + CT^{n_1}} - d_1[\mathrm{PKA}] \tag{2}$$

$$\frac{d[\mathrm{CREB}]}{dt} = \frac{V_2 \cdot [\mathrm{PKA}]}{K_2 + [\mathrm{PKA}]} - d_2[\mathrm{CREB}] \tag{3}$$

$$\frac{d[\mathrm{PI3K}]}{dt} = \frac{1}{1 + [\mathrm{PKA}]/K_3} - d_3[\mathrm{PI3K}] \tag{4}$$

$$\frac{d[\mathrm{AKT}]}{dt} = \frac{V_4 \cdot [\mathrm{PI3K}]}{K_4 + [\mathrm{PI3K}]} - d_4[\mathrm{AKT}] \tag{5}$$

$$\frac{d[\mathrm{pGSK3\beta}]}{dt} = \frac{V_5 \cdot ([\mathrm{GSK3\beta}_T] - [\mathrm{pGSK3\beta}])}{K_5 + [\mathrm{GSK3\beta}_T] - [\mathrm{pGSK3\beta}]} \cdot [\mathrm{AKT}] - d_5[\mathrm{pGSK3\beta}] \tag{6}$$

where $V_i$ and $K_i$ represent the maximal reaction rate and Michaelis constant of each protein mediated by its upstream regulator, respectively, and $n_i$ is a Hill coefficient. $a_1$ in Eq. (2) represents the base activation rate of PKA by cAMP. pGSK3β in Eq. (6) indicates the inactive, phosphorylated form of GSK3β, and $[\mathrm{GSK3\beta}_T]$ is total GSK3β. Hence, the active, unphosphorylated form of GSK3β [aGSK3β] is formulized as

$$[\mathrm{aGSK3\beta}] = [\mathrm{GSK3\beta}_T] - [\mathrm{pGSK3\beta}].$$

Active GSK3β can trigger cyclin D1 translocation and degradation; therefore, the degradation rate of cyclin D1 is dependent on GSK3β as described in the following function,

$$f_1([\mathrm{aGSK3\beta}]) = d_6 \cdot \frac{[\mathrm{aGSK3\beta}]}{K_{6b} + [\mathrm{aGSK3\beta}]} \cdot [\mathrm{Cyclin\ D1}].$$

Additionally, self-amplification or a positive feedback loop was assumed [8,17] for cyclin D1 to model its ultrasensitive response to graded changes of cholera toxin doses as indicated in the experimental data (Table S1). The self-amplification was described by the following non-linear Hill function,

$$f_2([\mathrm{Cyclin\ D1}]) = \frac{V_6 \cdot [\mathrm{Cyclin\ D1}]^{n_2}}{K_{6a}^{n_2} + [\mathrm{Cyclin\ D1}]^{n_2}}.$$

Therefore, the change rate of cyclin D1 balanced by its activation and degradation was modeled as follows,

$$\frac{d[\mathrm{Cyclin\ D1}]}{dt} = f_2([\mathrm{Cyclin\ D1}]) - f_1([\mathrm{aGSK3\beta}]). \tag{7}$$

Similarly, cAMP-dependent activation of the IL6-JAK2-STAT3 pathway induced by cholera toxin was described using Hill functions as below,

$$\frac{d[\mathrm{IL6}]}{dt} = \frac{V_7 \cdot [\mathrm{cAMP}]}{K_7 + [\mathrm{cAMP}]} - d_7[\mathrm{IL6}] \tag{8}$$

$$\frac{d[\mathrm{JAK2}]}{dt} = \frac{V_8 \cdot [\mathrm{IL6}]}{K_8 + [\mathrm{IL6}]} - d_8[\mathrm{JAK2}] \tag{9}$$

$$\frac{d[\mathrm{STAT3}]}{dt} = \frac{V_9 \cdot [\mathrm{JAK2}]}{K_9 + [\mathrm{JAK2}]} - d_9[\mathrm{STAT3}]. \tag{10}$$

GFAP is a reliable marker of glioma cell differentiation, which is dependent on the activation levels of CREB, STAT3 and active GSK3β. Additionally, the degradation of cyclin D1 is a prerequisite for the differentiation of glioma cells. We modeled the activation level of GFAP as follows,

$$\begin{aligned}\frac{d[\mathrm{GFAP}]}{dt} &= f_3([\mathrm{Cyclin\ D1}]) \\ &\cdot \left(\frac{V_{10ab} \cdot [\mathrm{CREB}]}{K_{10a} + [\mathrm{CREB}]} \cdot \frac{[\mathrm{STAT3}]}{K_{10b} + [\mathrm{STAT3}]} + \frac{V_{10c} \cdot [\mathrm{aGSK3\beta}]^{n3}}{K_{10c} + [\mathrm{aGSK3\beta}]^{n3}}\right) \\ &- d_{10}[\mathrm{GFAP}].\end{aligned} \tag{11}$$

where

$$f_3([\mathrm{Cyclin\ D1}]) = \left(\frac{C - [\mathrm{Cyclin\ D1}]}{C}\right)^{+}$$

with $C$ as the maximal value of the steady states of cyclin D1 and $(x)^{+} = \begin{cases} x, x > 0 \\ 0, x \leqslant 0 \end{cases}$.

Similarly, PCNA activation by cyclin D1 and STAT3 through the above pathways was modeled as

$$\frac{d[\mathrm{PCNA}]}{dt} = \frac{V_{11a} \cdot [\mathrm{Cyclin\ D1}]}{K_{11a} + [\mathrm{Cyclin\ D1}]} + \frac{V_{11b} \cdot [\mathrm{STAT3}]}{K_{11b} + [\mathrm{STAT3}]} - d_{11}[\mathrm{PCNA}]. \tag{12}$$

The methods of parameter estimation and sensitivity analysis were described in Text S1.

## Acknowledgements

We acknowledge Drs. Jun Cui and Tingzhe Sun for valuable discussions. This work was supported by Grants from the National Natural Science Foundation of China (Nos. 81202555 and 81373428), the Guangdong Nature Science Foundation (No. 2014A030310355) and the "985 project" of Sun Yat-sen University (No. 50000-31101302).

## Appendix A. Supplementary data

Supplementary data associated with this article can be found, in the online version, at http://dx.doi.org/10.1016/j.febslet.2015.07.014.

## References

[1] Yiu, G. and He, Z. (2006) Glial inhibition of CNS axon regeneration. Nat. Rev. Neurosci. 7, 617–627.
[2] Leszczyniecka, M., Roberts, T., Dent, P., Grant, S. and Fisher, P.B. (2001) Differentiation therapy of human cancer: basic science and clinical applications. Pharmacol. Ther. 90, 105–156.
[3] Li, Y. et al. (2007) Cholera toxin induces malignant glioma cell differentiation via the PKA/CREB pathway. Proc. Natl. Acad. Sci. 104, 13438–13443.
[4] Bao, S. et al. (2006) Glioma stem cells promote radioresistance by preferential activation of the DNA damage response. Nature 444, 756–760.
[5] Guerrant, R.L., Fang, G.D., Thielman, N.M. and Fonteles, M.C. (1994) Role of platelet activating factor in the intestinal epithelial secretory and Chinese hamster ovary cell cytoskeletal responses to cholera toxin. Proc. Natl. Acad. Sci. 91, 9655–9658.
[6] Li, Y. et al. (2010) Glycogen synthase kinases-3β controls differentiation of malignant glioma cells. Int. J. Cancer 127, 1271–1282.
[7] Shu, M. et al. (2011) Activation of a pro-survival pathway IL-6/JAK2/STAT3 contributes to glial fibrillary acidic protein induction during the cholera toxin-induced differentiation of C6 malignant glioma cells. Mol. Oncol. 5, 265–272.
[8] Gérard, C. and Goldbeter, A. (2009) Temporal self-organization of the cyclin/Cdk network driving the mammalian cell cycle. Proc. Natl. Acad. Sci. 106, 21643–21648.
[9] Yao, G., Lee, T.J., Mori, S., Nevins, J.R. and You, L. (2008) A bistable Rb–E2F switch underlies the restriction point. Nat. Cell Biol. 10, 476–482.
[10] Xiong, W. and Ferrell, J.E. (2003) A positive-feedback-based bistable 'memory module' that governs a cell fate decision. Nature 426, 460–465.
[11] Huang, C.-Y. and Ferrell, J.E. (1996) Ultrasensitivity in the mitogen-activated protein kinase cascade. Proc. Natl. Acad. Sci. 93, 10078–10083.
[12] Gardner, T.S., Cantor, C.R. and Collins, J.J. (2000) Construction of a genetic toggle switch in *Escherichia coli*. Nature 403, 339–342.
[13] Spencer, S.L. et al. (2013) The proliferation-quiescence decision is controlled by a bifurcation in CDK2 activity at mitotic exit. Cell 155, 369–383.
[14] Novak, B. and Tyson, J.J. (2008) Design principles of biochemical oscillators. Nat. Rev. Mol. Cell Biol. 9, 981–991.
[15] Mather, W., Bennett, M.R., Hasty, J. and Tsimring, L.S. (2009) Delay-induced degrade-and-fire oscillations in small genetic circuits. Phys. Rev. Lett. 102, 068105.
[16] Gonze, D. and Abou-Jaoudé, W. (2013) The Goodwin model: behind the Hill function. PLoS One 8, e69573.
[17] Swat, M., Kel, A. and Herzel, H. (2004) Bifurcation analysis of the regulatory modules of the mammalian G1/S transition. Bioinformatics 20, 1506–1511.
[18] Bliss, C. (1939) The toxicity of posons applied jointly. Ann. Appl. Biol. 26, 585–615.
[19] Fitzgerald, J.B., Schoeberl, B., Nielsen, U.B. and Sorger, P.K. (2006) Systems biology and combination therapy in the quest for clinical efficacy. Nat. Chem. Biol. 2, 458–466.
[20] Hitomi, M. and Stacey, D.W. (1999) Cellular ras and cyclin D1 are required during different cell cycle periods in cycling NIH 3T3 cells. Mol. Cell. Biol. 19, 4623–4632.
[21] Stacey, D.W. (2003) Cyclin D1 serves as a cell cycle regulatory switch in actively proliferating cells. Curr. Opin. Cell Biol. 15, 158–163.
[22] Sa, G. et al. (2002) Ras is active throughout the cell cycle, but is able to induce cyclin D1 only during G2 phase. Cell Cycle (Georgetown, Tex.) 1, 50–58.
[23] Guo, Y., Stacey, D.W. and Hitomi, M. (2002) Post-transcriptional regulation of cyclin D1 expression during G2 phase. Oncogene 21, 7545–7556.
[24] Musgrove, E.A., Caldon, C.E., Barraclough, J., Stone, A. and Sutherland, R.L. (2011) Cyclin D as a therapeutic target in cancer. Nat. Rev. Cancer 11, 558–572.
[25] Sun, X. et al. (2012) Multi-scale agent-based brain cancer modeling and prediction of TKI treatment response: Incorporating EGFR signaling pathway and angiogenesis. BMC Bioinformatics 13, 218.
[26] Sun, X. et al. (2013) Modeling vascularized bone regeneration within a porous biodegradable CaP scaffold loaded with growth factors. Biomaterials 34, 4971–4981.
[27] Sun, X. et al. (2012) Cytokine combination therapy prediction for bone remodeling in tissue engineering based on the intracellular signaling pathway. Biomaterials 33, 8265–8276.
[28] Leder, K. et al. (2014) Mathematical modeling of PDGF-driven glioblastoma reveals optimized radiation dosing schedules. Cell 156, 603–616.
[29] Heidari, P. et al. (2013) Free somatostatin receptor fraction predicts the antiproliferative effect of octreotide in a neuroendocrine tumor model: implications for dose optimization. Cancer Res. 73, 6865–6873.